JGR Earth Surface

Correspondence to:
S. Rezvanbehbahani,
soroushr@ku.edu

An Improved Analytical Solution for the Temperature Profile of Ice Sheets

Soroush Rezvanbehbahani[1,2] (iD), C. J. van der Veen[3] (iD), and Leigh A. Stearns[1,2] (iD)

[1]Department of Geology, University of Kansas, Lawrence, KS, USA, [2]Center for Remote Sensing of Ice Sheets, University of Kansas, Lawrence, KS, USA, [3]Department of Geography and Atmospheric Science, University of Kansas, Lawrence, KS, USA

Abstract The one-dimensional steady state analytical solution of the energy conservation equation obtained by Robin (1955, https://doi.org/10.3189/002214355793702028) is frequently used in glaciology. This solution assumes a linear change in surface velocity from a minimum value equal to minus the mass balance at the surface to zero at the bed. Here we show that this assumption of a linear velocity profile leads to large errors in the calculated temperature profile and especially in basal temperature. By prescribing a nonlinear power function of elevation above the bed for the vertical velocity profile arising from use of the Shallow Ice Approximation, we derive a new analytical solution for temperature. We show that the solution produces temperature profiles identical to numerical temperature solutions with the Shallow Ice Approximation vertical velocity near ice divides. We quantify the importance of strain heating and demonstrate that integrating the strain heating and adding it to the geothermal heat flux at the bed is a reasonable approximation for the interior regions. Our analytical solution does not include horizontal advection components, so we compare our solution with numerical solutions of a two-dimensional advection-diffusion model and assess the applicability and errors of the analytical solution away from the ice divide. We show that several parameters and assumptions impact the spatial extent of applicability of the new solution including surface mass balance rate and surface temperature lapse rate. We delineate regions of Greenland and Antarctica within which the analytical solution at any depth is likely within 2 K of the actual temperatures with horizontal advection.

1. Introduction

Variations in ice temperature affect the deformation rate by altering the rate factor several orders of magnitude (e.g., Hooke, 1981), as well as the occurrence of sliding when basal temperatures reach the melting point (e.g., Iken & Bindschadler, 1986). Therefore, robust estimation of ice sheet temperatures is essential for modeling of ice flow. The temperature fields of ice sheets can be calculated using a variety of numerical models (e.g., SICOPOLIS, Greve & Hutter, 1995; ISSM, Larour, Seroussi, et al., 2012; VarGlaS, Brinkerhoff & Johnson, 2013; PISM, Aschwanden et al., 2012). However, applying these models often requires computationally expensive simulations. In contrast, analytical temperature solutions are useful because (1) they are significantly easier to implement, (2) they serve as a validation tool for numerical models, (3) they facilitate analyzing the sensitivity of temperature profiles to various input parameters, and (4) they can provide efficient tools for initializing numerical ice sheet simulations (e.g., Adalgeirsdottir et al., 2014; Aschwanden et al., 2013).

The only analytical temperature solution widely used in glaciology is the Robin (1955) solution. Robin emphasizes that his model is suitable only for the "temperature distribution near the centre of an ice sheet." This model is often used as a "back-of-the-envelope" means for estimating basal temperatures (e.g., Anandakrishnan et al., 1998; Jezek et al., 2015; Palmer et al., 2013; Portnov et al., 2016; Siegert, 2000); however, there has been no attempt to validate or quantify uncertainties associated with this solution or define the area within which the Robin solution can be applied.

The Robin solution approximates the distribution of the vertical velocity as increasing linearly from the surface value, equal to minus the surface mass balance rate, to zero at the bed. Here we show that this assumption leads to an underestimation of temperatures, owing to extreme sensitivity of the energy conservation equation to parameterization of vertical velocity (section 2.1). In order to resolve this issue, we approximate the vertical velocity obtained from the Shallow Ice Approximation (SIA; Hutter, 1983) with a

Table 1
Symbols, Values, and Units

Symbol	Value	Unit	Description
A	5×10^{-8}	$kPa^{-3}year^{-1}$	deformation rate factor
$\dot{b}$		m/year	basal melt rate
c	2097	J/kg.K	heat capacity
erf(x)			error function
$\dot{\varepsilon}_{xz}$		year^{-1}	strain rate of vertical shear
G	50	mW/m^2	geothermal heat flux
G_s		mW/m^2	depth-integrated strain heating
γ			nonlinear exponent of vertical velocity
γ_+			optimal exponent
$\Gamma(a, x)$			upper incomplete gamma function
H		m	ice thickness
K	34.4	m^2/year	thermal diffusivity
κ	2.10	W/m.K	thermal conductivity
L		m	ice sheet length
L_f	333.5	kJ/kg	laten heat of fusion
$\dot{M}$		m/year	surface mass balance rate (ice equivalent)
n	3		Glen's flow law exponent
$\mathbf{n} = \{n_x, n_z\}$			normal vector
Q_s		mW/m^2	strain heating
ρ	910	kg/m^3	ice density
T		°C	temperature
T_s		°C	surface temperature
T_b		°C	basal temperature
τ_{dx}		kPa	driving stress
$\vec{v} = \{v_x, v_z\}$		m/year	horizontal and vertical velocity

power function of elevation above the bed. We then implement this velocity profile in the one-dimensional, steady state advection-diffusion equation and derive a new analytical solution that substantially improves the temperature estimates (sections 2.2 and 2.3).

The presented analytical solution does not include strain heating, and therefore, we evaluate its importance on the temperature profile (section 3). Additionally, we confirm the applicability of a previous suggestion of incorporating strain heating by adding the depth-integrated strain heating to the geothermal heat flux at the bed (Fowler, 1992) in the analytical solutions (section 3). Since the new analytical solution ignores horizontal heat advection, we also compare the temperatures from the analytical solution to that of a two-dimensional steady state ice sheet model, aiming at approximating the spatial extent away from the ice divide where our solution can be applied (section 4). Finally, the results, implications, and spatial extent of applicability to Greenland and Antarctic ice sheets are discussed (section 5).

2. One-Dimensional Models

In the interior of ice sheets, where horizontal velocities are small, the energy conservation can be considered in the vertical (z) direction only. That is, horizontal advection and diffusion of heat are assumed small and negligible. In steady state conditions, the 1-D energy conservation with constant heat flux at the bed (G) and constant temperature at the surface (T_s) for an ice thickness of H is (Van der Veen, 2013, Section 6.2)

$$-K\frac{\partial^2 T}{\partial z^2} + v_z\frac{\partial T}{\partial z} = \frac{Q_s}{\rho c}, \text{ for } z \in \Omega = (0, H) \tag{1a}$$

$$\frac{\partial T}{\partial n_z} = -\frac{G}{\kappa}, \text{ for } z \text{ on } \Gamma_N(z = 0) \tag{1b}$$

$$T = T_s, \text{ for } z \text{ on } \Gamma_D(z = H), \tag{1c}$$
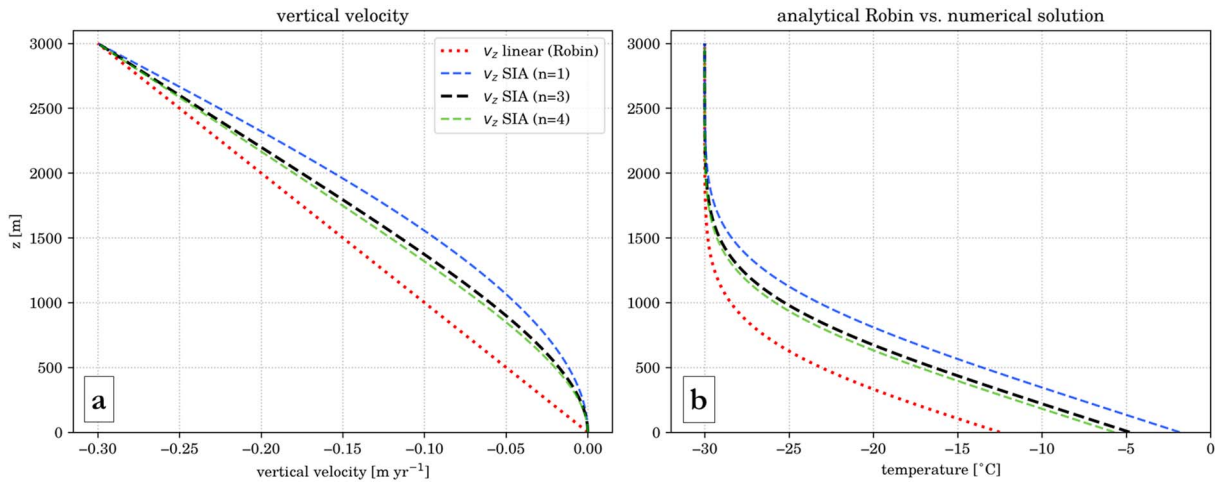
Figure 1. Parameterization of vertical velocities (a) and their corresponding temperature profiles (b) from the SIA (equation (4)) with different exponents of Glen's flow law and the Robin solution (equation (3)). The linear v_z from the Robin solution (*red dotted*) is compared with the exact vertical velocity from SIA (*dashed*). Surface mass balance rate, $\dot{M}$, is 0.3 m/year, and geothermal heat flux is G=50 mW/m². SIA = Shallow Ice Approximation.

where T is the ice temperature, K is thermal diffusivity, and κ is thermal conductivity; v_z is the vertical velocity; ρ and c are ice density and specific heat capacity, respectively. The surface and basal boundaries are denoted by Γ_D and Γ_N, while Ω refers to the ice column (minus the boundaries). The quantity **n** is the unit normal vector with components $\{n_x, n_z\}$ in horizontal and vertical directions, respectively. Symbols and their values are defined in Table 1.

In this study we initially ignore strain heating (Q_s) in the analytical derivation. We then include Q_s in the numerical solution and examine how it affects the temperature profile. We also evaluate a simple method to include strain heating in the analytical solution in section 3. Since we focus on nontemperate ice, the surface temperatures that we use are cold enough to ensure that the basal temperatures will not reach the pressure melting point throughout the study, and consequently, frictional heating arising from sliding at the bed can be ignored.

2.1. Accuracy of Robin's Analytical Solution

In the absence of basal melting, if the vertical ice velocity, v_z, is assumed to vary linearly from minus the surface mass balance rate, $-\dot{M}$, at the ice surface to zero at the bottom (with z axis positive upward), where the bed is at $z = 0$

$$v_z = -\frac{\dot{M}z}{H},$$ (2)

then the analytical solution obtained by Robin (1955) for ice temperature at a given depth reads

$$T(z) = T_s - \frac{G\sqrt{\pi}}{2\kappa q}[\text{erf}(zq) - \text{erf}(Hq)],$$ (3)

with $q = \sqrt{\frac{\dot{M}}{2KH}}$ and the error function is defined as $\text{erf}(z) = \frac{2}{\sqrt{\pi}}\int_0^z \exp(-z'^2)dz'$, where z' is a dummy variable. The basal temperature can be obtained by setting $z = 0$ in equation (3). Equation (2) holds when the bed is frozen, and therefore, basal vertical velocity is 0. However, extensions to the Robin solution have been proposed by Zotikov (1986, Section 4.2) and Hindmarsh et al. (2009) to include basal melt by introducing a nonzero vertical velocity at the bed in the analytical solution.

Robin's linear approximation for the vertical velocity does not substantially deviate from vertical velocities obtained by using the SIA. However, the system of equations (1a)–(1c) is very sensitive to the choice of vertical velocity distribution and inappropriate approximations lead to incorrect temperature estimates.

Using the SIA and further assuming that the surface vertical velocity equals the surface mass balance rate, the vertical velocity for $z \in (0, H)$ is (Hindmarsh, 1999),

$$v_{z_{\text{SIA}}} = -\frac{\dot{M}}{n+1}\left[\left(1 - \frac{z}{H}\right)^{n+2} - 1 + (n+2)\frac{z}{H}\right].$$ (4)

We use a finite element framework, FEniCS (Logg et al., 2012), to solve equation (1) numerically, given the SIA vertical velocity profile for equation (4). Comparison of the numerical temperature solution with that of the Robin solution (Figure 1) shows that small differences in the vertical velocity distribution can lead to the underestimation of the basal temperature by ~8 K in the Robin solution. This is because the linear velocity profile systematically overestimates the vertical velocity at depth and thus overestimates the downward advection of colder ice from the surface to deeper ice layers. Therefore, the Robin solution must be cautiously used as a back-of-the-envelope method to estimate temperature in the interior regions. In the following section, we address this issue by proposing a new analytical solution to equation (1). Note that in reality, warmer, less viscous ice near the bed (produced by the geothermal heat flux) changes the profile from the form of (4) to more resemble the Robin solution profile (2), reducing the numerical error associated with the Robin solution. However, simulating this process requires thermomechanical coupling, which is not considered in the Robin or the present solution.

2.2. New Analytical Temperature Solution

Assuming $n = 3$, the vertical velocity profile in the SIA (equation (4)) is a fifth-order polynomial. Deriving an analytical solution for the temperature profile in equation (1) using this equation is not straightforward and may not be possible. However, equation (4) can be approximated with a similar form to that of the Robin's approximation but with an exponent greater than unity for the z/H term so as to introduce a concavity to the vertical velocity profile, similar to that produced by modeling internal deformation using the SIA (Figure 1). Thus

$$v_z = -\dot{M}\left(\frac{z}{H}\right)^{\gamma}. \tag{5}$$

To find an analytical solution to the temperature equation (1) using this form for the velocity profile, we follow the classic procedure for solving second-order ordinary differential equations without the source term outlined by, for example, Boyce et al., (1969, Chapter 3).

Substituting profile (5) in equation (1) and for now setting Q_s to 0, the 1-D advection-diffusion equation becomes

$$\frac{\partial^2 T}{\partial z^2} + \frac{\dot{M}}{KH^{\gamma}}z^{\gamma}\frac{\partial T}{\partial z} = 0. \tag{6}$$

Next, we define λ as

$$\lambda = \frac{\dot{M}}{KH^{\gamma}}. \tag{7}$$

The heat equation can then be written as

$$\frac{\partial^2 T}{\partial z^2} + \mathcal{P}(z)\frac{\partial T}{\partial z} = 0, \tag{8}$$

where $\mathcal{P}(z) = \lambda z^{\gamma}$.

We define the temperature gradient term as $\frac{\partial T}{\partial z} = \psi(z)$, so that the heat equation becomes

$$\frac{\partial \psi(z)}{\partial z} + \mathcal{P}(z)\psi(z) = 0. \tag{9}$$

The solution of the function $\psi(z)$ is (Boyce et al., 1969, Chapter 3)

$$\psi(z) = \frac{C_1}{\mu(z)}, \tag{10}$$

where $\mu(z)$ is the integrating factor defined as

$$\mu(z) = \exp\left(\int \mathcal{P}(z)dz\right) = \exp\left(\int \lambda z^{\gamma} dz\right) = \exp\left(\frac{\lambda}{\gamma+1}z^{\gamma+1}\right). \tag{11}$$

At the ice sheet bed, $\psi(z) = \frac{\partial T}{\partial z}\big|_{z=0}$ represents the geothermal flux boundary condition on a flat bed (equation (1b)).

$$\psi(0) = \frac{C_1}{\mu(0)} = -\frac{G}{\kappa}. \tag{12}$$

From equation (11) we know that $\mu(0) = 1$, meaning that $C_1 = -\frac{G}{\kappa}$ and the full expression for $\psi(z)$ is

$$\psi(z) = \frac{-\frac{G}{\kappa}}{\mu(z)} = -\frac{G}{\kappa} \exp\left(-\frac{\lambda}{\gamma+1} z^{\gamma+1}\right). \tag{13}$$

Then, by defining $\phi = -\frac{\lambda}{\gamma+1}$, the temperature profile $T(z)$ can be obtained by integrating $\psi(z)$ as

$$T(z) = \int \psi(z)\mathrm{d}z = -\frac{G}{\kappa} \int \exp\left(\phi z^{\gamma+1}\right) \mathrm{d}z. \tag{14}$$

Therefore, the general solution to the temperature profile is

$$T(z) = -\frac{G}{\kappa} \left(\frac{-z\left(-\phi z^{\gamma+1}\right)^{\frac{-1}{\gamma+1}}}{\gamma+1} \right) \Gamma\left(\frac{1}{1+\gamma}, -\phi z^{\gamma+1}\right) + C_2. \tag{15}$$

where $\Gamma(\cdot,\cdot)$ is the upper incomplete gamma function (also known as the Euler integral of second kind) defined by Boyce et al., (1969, Chapter 6) as

$$\Gamma(a,x) = \int_x^\infty t^{a-1} e^{-t} \mathrm{d}t. \tag{16}$$

The value of $\Gamma(\cdot,\cdot)$ can be found in ordinary differential equation textbooks or standard numerical tables (e.g., Abramowitz & Stegun, 1964), as well as in several standard software packages, for example, NAG®, MATLAB®.

The integration constant, C_2, is found by setting $T(H)$ equal to the surface temperature, T_s. Substitution of this into equation (15) produces

$$T(z) = T_s + \frac{G(-\phi)^{\frac{-1}{\gamma+1}}}{\kappa(\gamma+1)} \left[\Gamma\left(\frac{1}{1+\gamma}, -\phi z^{\gamma+1}\right) - \Gamma\left(\frac{1}{1+\gamma}, -\phi H^{\gamma+1}\right) \right]. \tag{17}$$

Equation (17) is a general form of the analytical steady state solution to the 1-D energy equation with a prescribed heat flux at the bed, surface temperature T_s, and a velocity parameterization of the form $-\dot{M}(\frac{z}{H})^\gamma$ with $\gamma > 0$. In the special case where $\gamma = 1$, the error function emerges from the upper incomplete gamma function through $\mathrm{erf}(x) = 1 - \frac{\Gamma(\frac{1}{2}, x^2)}{\sqrt{\pi}}$ (Amore, 2005; Gautschi, 1998) and the Robin solution is reproduced. The difference between basal and surface temperature can be obtained by setting $z = 0$ in equation (17):

$$T_b - T_s = \frac{G(-\phi)^{\frac{-1}{\gamma+1}}}{\kappa(\gamma+1)} \left[\Gamma\left(\frac{1}{1+\gamma}, 0\right) - \Gamma\left(\frac{1}{1+\gamma}, -\phi H^{\gamma+1}\right) \right]. \tag{18}$$

The value of γ that produces the best fit for approximating the vertical velocity profile obtained from the SIA (equation (4)) is $\gamma = 1.397$. However, comparing the temperature profile calculated with this value in the analytical solution with the temperature profile obtained numerically (with the vertical velocity profile given by equation (4)) shows that the analytical solution does not quite match the numerical solution with $\gamma = 1.397$. Further adjustment of γ is required to match the temperature profile from analytical solution with that of the numerical solution.

To find the optimal γ (hereafter γ_+), we plot temperature profiles from the analytical solution for a range of γ values in order to match this solution with the numerical solution (Figure 2). For the specific case shown in Figure 2 (i.e., $\dot{M}=0.3$ m/year and $H = 3,000$ m), we find that $\gamma_+=1.523$. However, γ_+ depends upon surface mass balance rate and thickness values, which is investigated in section 2.3.
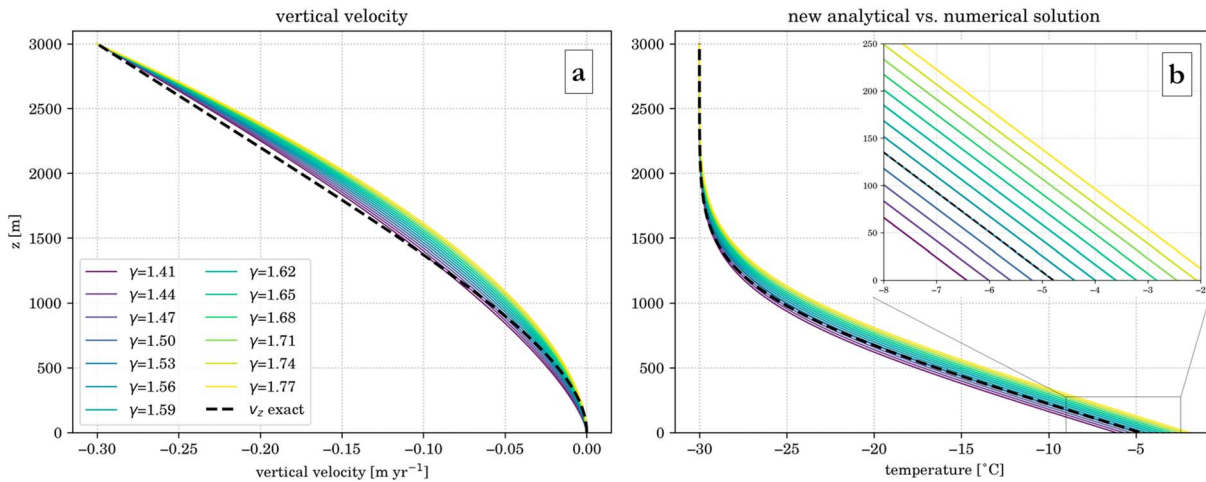
Figure 2. Parameterization of vertical velocity with different exponents (a) and their corresponding temperature profiles (b). The exact v_z from the Shallow Ice Approximation (equation (4), *dashed black*) is compared with nonlinear power functions. A range of γ values are used to estimate velocities (*colored lines*). In this specific case, $\gamma = 1.532$ shows the optimal exponent to match temperature calculations from our solution with that of Shallow Ice Approximation exact vertical velocities (inset). $\dot{M}$ is 0.3 m/year.

2.3. Finding γ_+

We perform a series of experiments to investigate parameters that affect γ_+. We find that γ_+ is sensitive to surface mass balance rate ($\dot{M}$) and ice thickness (H). Since $\dot{M}$ has the unit of velocity, the vertical Péclet number can be defined as $Pe = \frac{\dot{M}H}{K}$ (hereafter we drop "vertical"). The Péclet number is a nondimensional number that represents the ratio of advective to diffusive heat transfer (Bergman et al., 2011, Section 6.6). The vertical temperature distribution of the ice sheet strongly depends on Pe number. If $Pe = 0$ (i.e., no vertical advection), the vertical temperature distribution becomes linear with slope determined by the geothermal heat flux. In steady state conditions with large Pe, advective heat transfer dominates the upper part of the ice sheet, causing the upper layers to become isothermal (equal to the surface temperature), while the lower parts of the column will be mostly modulated by conductive heat transfer forming a conductive boundary layer near the bottom (Cuffey & Paterson, 2010; Zotikov, 1986). The normalized thickness of the conductive boundary layer near the bottom is $Pe^{-1/3}$ for the case of internal shearing and $Pe^{-1/2}$ for plug flow (Morland, 1984).

The range of Péclet numbers considered here is between ~2 and 100, corresponding to $\dot{M}$ values from 0.1 to 1.5 m/year and thickness values from 1,000 to 3,000 m (e.g., Van den Broeke et al., 2011). In the thick interior regions of ice sheets, vertical velocity as measured by the Péclet number is often insubstantial. For example, in the East Antarctic Ice Sheet the Péclet number lies between 2 and 4. Although Pe values as high as 100 are atypical in Greenland and Antarctica, they can occur in ice caps of Iceland or Antarctic Peninsula. We include this wide range of Pe numbers for completeness.

In order to find the γ_+, we iteratively solve for the γ in equation (18) with a fixed surface temperature T_s, in order to match the basal temperature from the analytical solution with the numerical solution. The iteration is terminated when the difference between basal temperatures from the two models is less than 0.05 K. Results are summarized in Figure 3 where γ_+ is shown to have a logarithmic relationship with Péclet number as

$$\gamma_+ = 1.39 + 0.044 \ln(Pe). \tag{19}$$

Hereafter, all the calculations from the analytical solution are with γ_+ obtained from equation (19), unless otherwise specified. Note that since our analysis is thermomechanically decoupled, the vertical velocity distribution is independent of the ice temperature. Therefore, the value of γ_+ does not vary with changing T_s or G.

3. Effect of Strain Heating

The analytical solution (17) is obtained in the absence of strain heating in (1). Since strain heating is a depth-dependent term, it cannot be easily incorporated in the analytical solution. However, because most
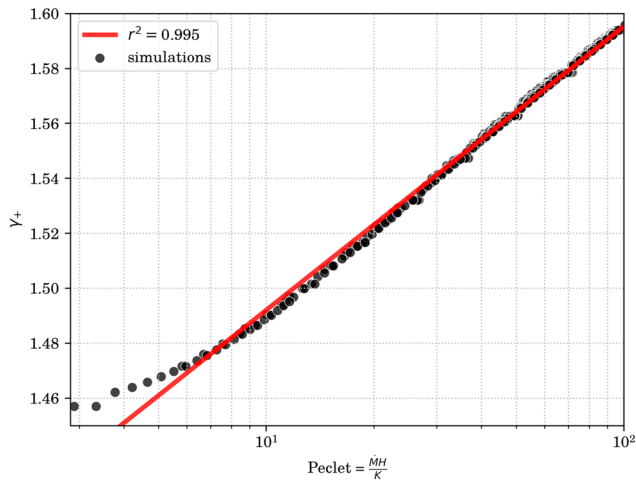
Figure 3. Dependence of γ_+ on vertical Pe. The value for γ_+ is calculated by iterative adjustment of γ in our solution to match the numerical solution (*black circles*), and the logarithmic fit (*red line*) provides an expression for finding the optimal gamma value. The value of γ_+ is independent of basal and surface boundary conditions (G and T_s).

of the vertical shear is concentrated in the basal ice layers, Fowler (1992) suggests that a good approximation is that the strain heating can be included by adding it to the basal boundary condition (equation (1b)). In this section, we investigate under which conditions this "lumping" of strain heating to the basal boundary condition is valid, by comparing the basal temperatures estimated from the analytical solution with those obtained from the numerical solution (which includes explicit calculation of strain heating at depth).

Heat released by internal deformation of ice can be expressed in terms of vertical shear strain rate ($\dot{\epsilon}_{xz}$) and shear stress (τ_{xz}) at depth through (e.g., Van der Veen, 2013, Section 4.2)

$$Q_s = 2\dot{\epsilon}_{xz}\tau_{xz}. \tag{20}$$

This equation is a valid approximation when SIA constraints hold. For lamellar flow the shear stress increases linearly from 0 at the surface to maximum shear stress at the bed. In case of SIA, the basal shear stress equals the driving stress, which is calculated by $\tau_{dx} = -\rho g H \frac{\partial H}{\partial x}$ (Nye, 1952). Applying Glen's constitutive relation with $n = 3$, and rate factor A to express the vertical strain rate in terms of the shear stress, the strain heating at depth becomes (Blatter & Greve, 2015; Van der Veen, 2013),

$$Q_s = 2A\left(1 - \frac{z}{H}\right)^4 \tau_{dx}^4. \tag{21}$$

If the temperature is solved numerically, this term can be added explicitly at every depth (note that dependence of rate factor, A, on temperature is neglected). However, including the source term in the form of equation (21) in the 1-D energy conservation equation would further complicate the analytical temperature solution, if a solution exists at all. Therefore, we evaluate whether the strain heating can be incorporated by elevating the heat flux at the bed. The total strain heating in an ice column (G_s) can be obtained by integrating equation (21) along a vertical profile; therefore,

$$G_s = \int_0^H Q_s dz = \int_0^H 2A\left(1 - \frac{z}{H}\right)^4 \tau_{dx}^4 dz = \frac{2}{5}AH\tau_{dx}^4. \tag{22}$$

This amount of strain heating needs to be added to the basal boundary condition used in the analytical solution.

To assess the importance of strain heating for temperature of an ice column, we compare temperature profiles from (1) temperature profile from the analytical solution without strain heating, (2) temperature profile from the analytical solution with G_s added to the geothermal heat flux, and (3) numerical solution with Q_s as strain heating at depth. The ice thickness is 3,000 m with T_s of $-30°C$, $\dot{M}$ of 0.3 m/year (which results in $Pe = 26.16$) and G of 50 mW/m². Since strain heating depends on rate factor and driving stress, different values of rate factor are chosen to represent the effect of hard and soft ice, in addition to three driving stress values (Figure 4). The three driving stress values of 20, 40, and 60 kPa are chosen as typical values in the interior regions of ice sheets (see Figure 1 in Sergienko et al., 2014).

Our results indicate that for low driving stresses ($\sim$20 kPa), regardless of the rate factor, the effect of strain heating is negligible, and all three profiles (with different rate factors) produce nearly identical temperatures (Figures 4a, 4d, and 4g). At a driving stress of 40 kPa, temperature estimates from both the numerical inclusion of strain heating (Q_s) and the "lumped" strain heating (G_s) increase, with the lumped strain heating slightly overestimating the basal temperatures compared with the numerical solutions. For a soft ice with the rate factor of 10^{-7} kPa^{-3}/year (corresponding to $\sim -5°C$), the basal temperature with G_s exceeds that of Q_s by less than 2 K. However, ignoring the strain heating underestimates the basal temperature by about $\sim$4 K (Figure 4h). With the driving stress of 40 kPa, these two approaches of including the strain heating (i.e., Q_s and G_s) produce relatively similar temperature profiles, confirming the previous suggestion by Fowler (1992). With the driving stress of 60 kPa, temperature overestimation of the
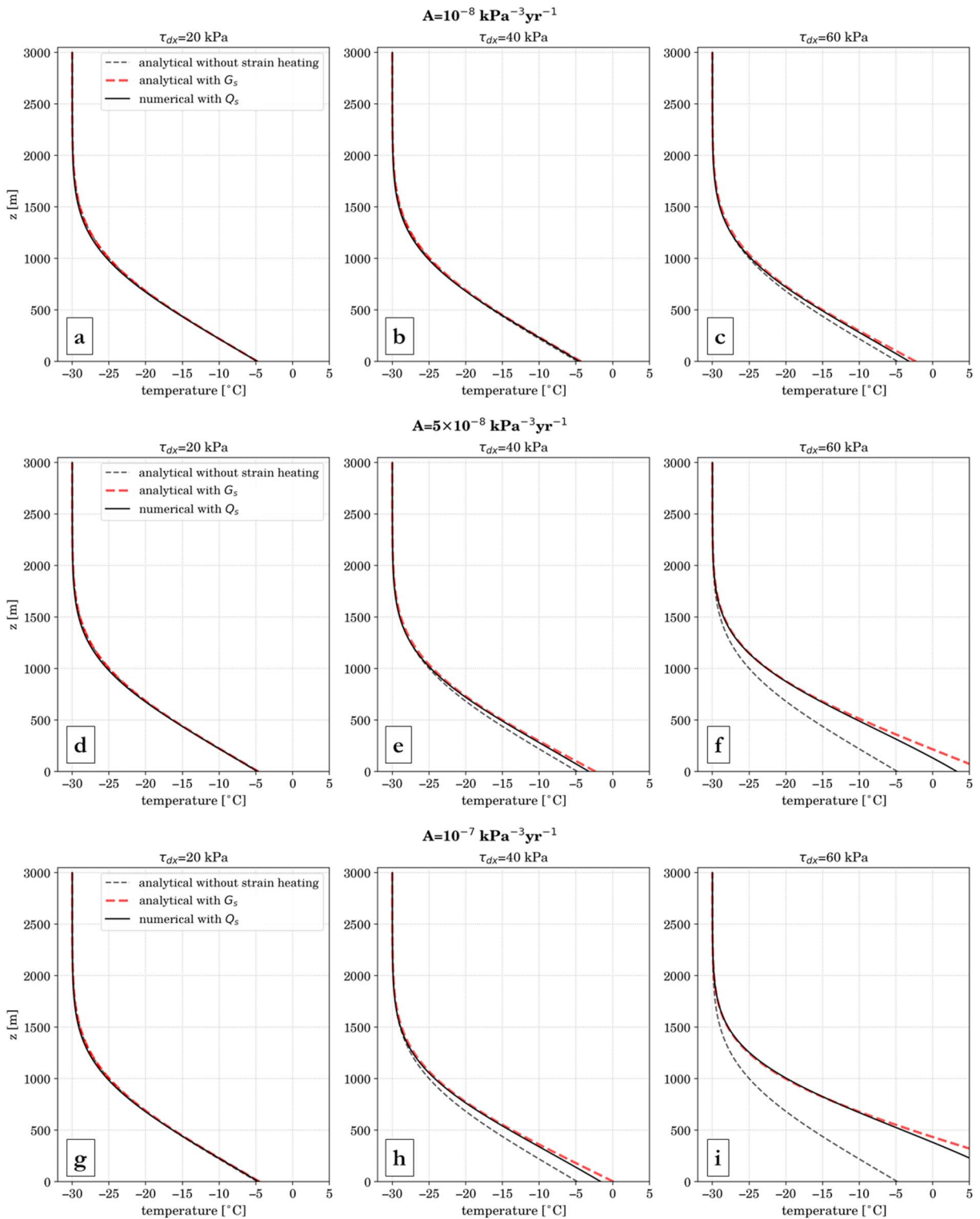
Figure 4. (a–i) Incorporating strain heating in the temperature profile. The analytical solution without strain heating (*dashed gray*) is compared with the numerical solution with strain heating (*solid black*) and addition of depth-integrated strain heating to the geothermal heat flux in the analytical solution (*dashed red*). Temperature profiles at each row have the same rate factor that correspond to −20, −10, and −5°C, respectively.
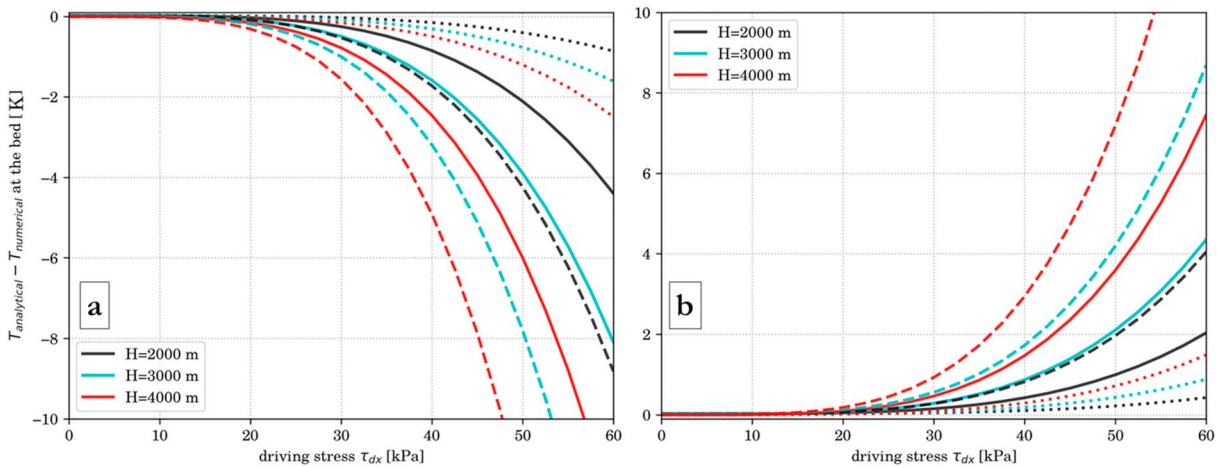
Figure 5. Effect of strain heating on the basal temperature of an ice column with varying ice thickness and rate factors. (a) The difference between basal temperature from the analytical solution without strain heating and the numerical solution with strain heating, and (b) The same temperature difference but depth-integrated strain heating is added to the heat flux at the bed. In the numerical solution, strain heating expression (Q_s, equation (21)) is incorporated as a source term in the solution (right-hand side of equation (1)). For the analytical solution the depth-integrated strain heating (G_s, equation (22)) is added to the geothermal heat flux of 50 mW/m^2 at the bottom. Results are shown for three different values of rate factor as $A = 10^{-8}$ (*dotted*), $A = 5 \times 10^{-8}$ (*solid*), and $A = 10^{-7}$ kPa^{-3}/year (*dashed*) lines. Note the difference in y axes.

lumped strain heating compared with the numerical inclusion of Q_s is small for a hard ice with a rate factor of 10^{-8} kPa^{-3}/year (Figure 4c). However, this overestimation rapidly increases for softer ice with rate factors of 5×10^{-8} and 10^{-7} kPa^{-3}/year, making the lumping method less accurate (Figures 4f and 4i).

Since both G_s and Q_s are related to the fourth power of driving stress, the significance of including strain heating (either through G_s or Q_s) sharply increases with increase in driving stress. Therefore, ignoring the strain heating in the analytical solution results in erroneous underestimation of temperature profile. Although the lumping method suggested by Fowler (1992) slightly overestimates the basal temperature compared with the numerical inclusion of Q_s, the magnitude of its overestimation is significantly smaller than the magnitude of underestimation when strain heating is ignored.

Figure 5 shows a similar comparison to that in Figure 4 but for basal temperatures of ice columns with different thickness and rate factors. For a hard ice with rate factor of 10^{-8} kPa^{-3}/year (corresponding to $\sim -20°C$) ignoring strain heating results in underestimation of basal temperature in the analytical solution by ~ 2 K. For softer ice the underestimation becomes more marked and rapidly increases with larger driving stress values (Figure 5a). However, lumping the depth-integrated strain heating with geothermal heat flux, despite the slight overestimation of basal temperature compared with the numerical solution with Q_s, produces a more reliable approximation of the basal temperature. Although the difference between the analytical and numerical solutions (with G_s and Q_s, respectively) increases with driving stress (Figure 5b), the difference in basal temperatures remains within ~ 2 K up to driving stress of ~ 50–60 kPa. Ignoring the strain heating in the analytical solution, however, results in substantial underestimation of basal temperatures even with small driving stresses and rate factors (Figure 5a). Therefore, our results corroborate the findings of Fowler (1992) and G_s obtained from equation (22) must be incorporated in the analytical solution.

Note that a uniform rate factor over the depth of the ice column has been used throughout this study. The rate factor is, however, a temperature-dependent parameter, but that is not considered here. In order to properly account for the changes of rate factor, the energy equation must be solved numerically by parameterizing the rate factor as a function of temperature (e.g., Clarke et al., 1977), which is not included in this study.

Although the driving stress is 0 at the ice divide (and strain heating is consequently 0), our temperature solution does not accurately estimate the basal temperature at the ice divide locations. Since the basal shear stress becomes 0 at the ice divide, the SIA assumptions are violated, and therefore, the vertical velocity shape function at the ice divide is different from the SIA-derived vertical velocity (Raymond, 1983). Our solution incorporates an approximation to the SIA-derived vertical velocity profile, and therefore, it cannot be used at the ice divide where SIA assumptions are violated (see section 5 for discussion).
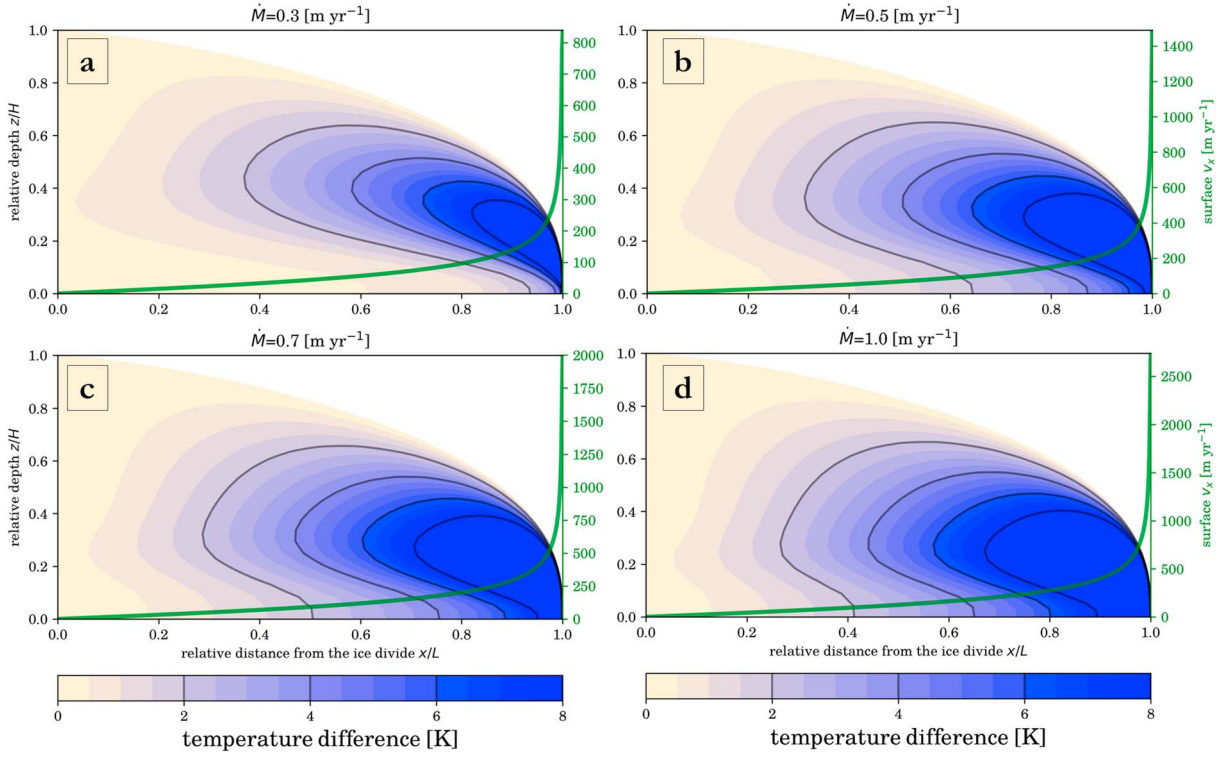
Figure 6. (a–d) Difference between the analytical solution and the full 2-D solution ($T_{\text{analytical}} - T_{\text{numerical}}$) for a Vialov profile with different $\dot{M}$ values and geothermal heat flux of $G = 50$ mW/m^2. The analytical solution is calculated using γ_+ as a function of Péclet number (equation (19)). Surface temperature lapse rate of 7.1 K/km is used as an average annual value representing Greenland (Steffen & Box, 2001). Contour lines representing 2k intervals are shown (*solid black*). The second y axis shows the surface horizontal velocity of the Vialov profile (*green line*).

4. Effect of Horizontal Advection

Since the upstream high-elevation regions have a colder surface temperature (owing to temperature lapse rates being negative), the ice that is advected downstream has a lower temperature than the ice deposited immediately above. Hence, the horizontal ice flow lowers the temperature of the downstream regions. Since equation (17) is derived as a solution of the 1-D temperature equation and ignores the effect of horizontal heat advection, we compare temperatures from our solution with those obtained numerically for a two-dimensional ice sheet. As with the one-dimensional numerical solutions, we use FEniCS to solve the temperature equation:

$$-K\left(\frac{\partial^2 T}{\partial z^2} + \frac{\partial^2 T}{\partial x^2}\right) + \left(v_z \frac{\partial T}{\partial z} + v_x \frac{\partial T}{\partial x}\right) = 0, \text{ on } \Omega, \tag{23a}$$

$$\frac{\partial T}{\partial n_z} = -\frac{G}{\kappa}, \text{ for } z \text{ on } \Gamma_{N_1}(z = 0), \tag{23b}$$

$$\frac{\partial T}{\partial n_x} = 0, \text{ for } x \text{ on } \Gamma_{N_2}(x = 0), \tag{23c}$$

$$T = T_s, \text{ for } z \text{ on } \Gamma_D(z = H), \tag{23d}$$

with Γ_{N_1} denoting the basal boundary and Γ_{N_2} denoting the boundary at the ice divide. We apply a range of surface mass balance and temperature lapse rates for 2-D simulations with surface temperature of $-20°$C at zero elevation, chosen sufficiently low to keep basal temperatures below the pressure melting point. Strain heating is also ignored for 2-D simulations.

For the ice sheet profile, we use the Vialov (1958) steady state profile, which is based on horizontal ice velocity determined by the SIA and constant surface mass balance rate. The Vialov profile is

$$\left(\frac{H}{H_0}\right)^{2+\frac{2}{n}} + \left(\frac{x}{L}\right)^{1+\frac{1}{n}} = 1, \tag{24}$$
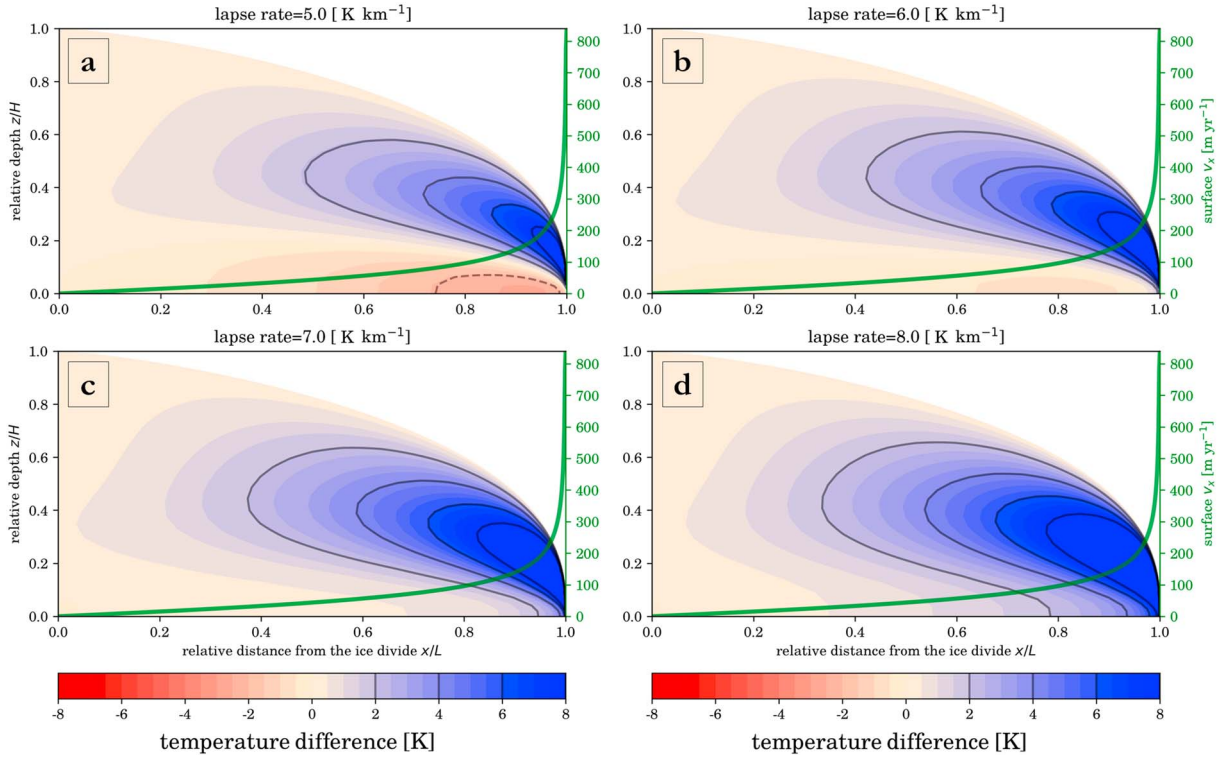
Figure 7. Same as Figure 6 but with different values for surface temperature lapse rates. The $\dot{M}$ of 0.3 m/year is used in the Vialov profile, and geothermal heat flux is $G = 50$ mW/m^2.

with thickness at the ice divide, H_0, defined as

$$H_0^{2+\frac{2}{n}} = 2\left(\frac{\dot{M}}{A_0}\right)^{\frac{1}{n}} L^{1+\frac{1}{n}}, \tag{25}$$

and the constant A_0 defined as

$$A_0 = \frac{2A}{n+2}(\rho g)^n. \tag{26}$$

Since the ice thickness goes to 0 at the edge of the Vialov profile, we artificially assign a thickness of 5 m to the downstream edge of the profile to prevent singularity in the continuity equation. We adopt the Vialov profile to avoid introducing too many variables and feedbacks. The two-dimensional temperature equation (23) is solved numerically for this profile. The artificially modified 5-m thickness at the edge of the profile has a constant temperature boundary condition of $-20°$C.

The Vialov profile (equation (24)) is calculated for an ice sheet of length $L = 750$ km and rate factor of $A = 5 \times 10^{-8}$ kPa^{-3}/year, roughly corresponding to $-10°$C temperature. The uniform rate factor implies that we are not accounting for thermomechanical coupling between temperature and ice flow (similar to section 3). We use different surface mass balance rates between 0.3 and 1 m/year. After obtaining the surface profile and driving stress through $\tau_{dx} = -\rho g H \frac{\partial H}{\partial x}$, we calculate the horizontal and vertical velocities $\{v_x, v_z\}$ from the SIA (Van der Veen, 2013, equations (4.22)–(4.30)). We then apply the calculated velocities into the 2-D energy conservation equation (23) and solve for the temperature distribution using the Galerkin finite element method. The streamline upwind Petrov-Galerkin method (Brooks & Hughes, 1982) is implemented to stabilize the spurious oscillations arising from the advection terms (similar to Brinkerhoff & Johnson, 2013; Cummings, 2016).

So far in the analysis, the surface kinematical condition has been equating the surface vertical velocity to $-\dot{M}$. While this is a reasonable approximation close to the ice divide, farther away, the effect of surface slope on the kinematical condition has to be accounted for. For steady state conditions, the vertical velocity at
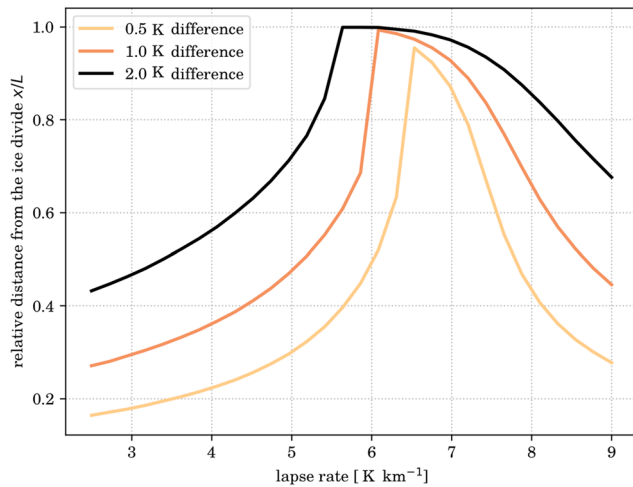
Figure 8. The basal temperature difference between the analytical solution and 2-D numerical solution as a function of surface temperature lapse rate. The x axis shows the range of lapse rates, and the y axis is the maximum normalized distance from the ice divide where the difference between the two solutions is less than defined temperature thresholds. At lapse rates lower than where the peak occurs, our analytical solution overestimates the basal temperatures and vice versa. $\dot{M}$ of 0.3 m/year and G of 50 mW/m² are used for simulations.

the surface is related to the mass balance and horizontal velocity at the surface as (Van der Veen, 2013, equation (9.77)),

$$v_z|_{\text{surface}} = v_x|_{\text{surface}} \frac{\partial H}{\partial x} - \dot{M}. \tag{27}$$

The surface vertical velocities are calculated from equation (27) and applied in the analytical solution.

We present a series of comparisons between our analytical solution and the 2-D thermal model. For clarity, only one parameter is changed at a time. Figure 6 shows the difference between the analytical and the numerical solution for a range of surface mass balance rates with a lapse rate of 7.1 K/km (the annual average for Greenland, Steffen & Box, 2001). A new Vialov profile and corresponding SIA velocity fields are calculated for every surface mass balance rate, and the surface horizontal velocity along the ice sheet is plotted over the Vialov profile (Figure 6). This comparison shows that the 1-D analytical solution overestimates englacial temperatures away from the ice divide (owing to the absence of horizontal advection terms). However, the basal temperature differences remain within 1−2 K for a large portion of the distance from the ice flow center. Use of the SIA in the creation of the Vialov profile shows that the horizontal velocities increase with an increase in the surface mass balance rate. Hence, the effect of horizontal advection lowers the downstream temperatures (as shown in Figure 6). Although the location of the 2 K offset in basal temperatures varies with changes in $\dot{M}$ values, the magnitude of surface velocities remains between ∼100 and 200 m/year for all profiles (Figure 6).

We assess the effect of surface temperature lapse rate on horizontal heat advection. We use a range of lapse rates from 5 to 8 K/km to a Vialov profile with $\dot{M}$ of 0.3 m/year (Figure 7). Since the surface mass balance rate is taken uniform for all comparisons, velocities for all simulations are identical and surface temperature is the only different parameter between these simulations. With a lower lapse rate of 5 K/km our solution slightly overestimates the basal temperature farther from the ice divide. As the lapse rate increases, the colder ice advected from upstream regions increases and shortens the extent of our 1-D solution's applicability within a 2-D Vialov profile. The surface horizontal velocity at the location where the offset in basal temperatures is 2 K is ∼100 m/year (similar to Figure 6).

We summarize the results of experiments with different lapse rates in Figure 8, which shows the maximum normalized distance from the ice divide where the difference between the basal temperatures from the two solutions less than a defined threshold. The thresholds, arbitrarily defined at 0.5, 1, and 2 K, are plotted with respect to the range of lapse rates. The extents of applicability show a notable peak at certain lapse rates, below which the analytical solution overestimates and above which it underestimates the basal temperature profiles. For lapse rates between 5.5 and 7.5 K/km, the difference in basal temperature estimates is small for much of the ice sheet length. However, for low lapse rates of 3–4 K/km and lapse rates larger than 8 K/km, the extent of applicability of the 1-D analytical solution is more limited.

5. Discussion

We have presented a new analytical solution to the 1-D vertical heat transport equation with flow field constrained by the SIA by parameterizing the vertical velocity of the SIA as a power function. In the absence of horizontal velocities, the temperatures from the new analytical solution match those from the numerical solution with the exact SIA vertical velocity. The analytical solution incorporates an optimal exponent, γ_+, which depends on surface mass balance rate, $\dot{M}$, and thickness of the ice column, H. In order to use this solution, one must first calculate the vertical Péclet number as $Pe = \frac{\dot{M}H}{K}$ and use it to obtain γ_+ (equation (19)). The value of γ_+ can be used to calculate the temperature profile using equation (17), and basal temperature can be obtained through equation (18). In order to include the strain heating in the analytical solution, the depth-integrated strain heating obtained from equation (22) can be added to the geothermal heat flux at the bed (following Fowler, 1992).
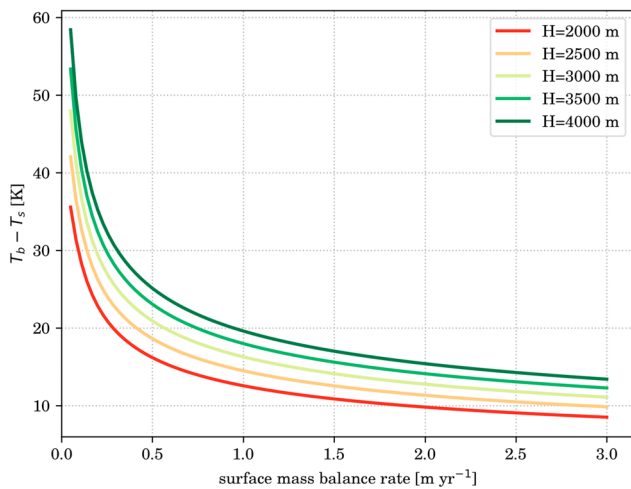
Figure 9. Difference between basal and surface temperature ($T_b - T_s$) from the analytical solution (equation 18) with respect to surface mass balance rate near ice divide for different thickness values.

The Péclet number includes the effects of two parameters that have an opposite effect on the temperature of an ice column: ice thickness has an insulating effect, so that thicker ice results in warmer temperatures at depth, while increase in surface mass balance rate results in increased vertical advection of cold surface ice, lowering the temperature at depth. According to equation (19), γ_+ increases with an increase in $\dot{M}$, and higher γ_+ results in warmer temperature profiles (Figure 2). This may appear contradictory because surface mass balance acts as a cooling agent. However, the magnitude of γ_+ increases marginally with an increase in $\dot{M}$, while changes in ϕ and $\Gamma(\cdot, \cdot)$ in the analytical solution (equation (17)) cancel the small increase in basal temperature due to increased γ_+. Therefore, the analytical solution is robust in capturing the thermal effect of increased vertical advection. This is evident in Figure 9, where larger surface mass balance rates reduce the difference between surface and basal temperature hence cooling the temperature profile, while the $T_b - T_s$ increases with an increase in ice thickness.

Note that at close proximity to ice divides (i.e., a few ice thicknesses) the basal shear stress becomes zero, violating SIA assumptions (Raymond, 1983) and having the consequence of inducing formation of a stagnant plug near the base under the divide. Also, it has been suggested that Glen's flow exponent near ice divides is close to 1 (Pettit & Waddington, 2003), which also results in lower rate of vertical advection of cold ice and leads to a warmer basal ice (Figure 1, blue curves). Therefore, our analytical solution likely underestimates the basal temperatures in a region about ~3–4 ice thicknesses away from ice divides.

In all comparisons, the parameters of interest are kept uniform along the ice flow. This is certainly an oversimplification; surface mass balance clearly is not uniform on the ice sheet with higher rates near the margins than the interiors (e.g., Ettema et al., 2010), and spatial variations of geothermal heat flux (e.g., Fox Maule et al., 2009; Rezvanbehbahani et al., 2017) have been shown to significantly impact the velocity field of ice sheets (e.g., Larour, Morlighem, et al., 2012; Schlegel et al., 2015). Surface temperature lapse rate is also unlikely to be uniform along the surface of an ice sheet (e.g., Erokhina et al., 2017; Hanna et al., 2005), which can alter the ice sheet temperature distribution. In the present study, the Vialov profiles and the corresponding velocities are obtained from an ice sheet-wide uniform rate factor, and the mechanical model is decoupled from the thermal model. The interaction between the flow regime and thermal field requires thermomechanical coupling, which is not included and is beyond the scope of this study (see, e.g., Bondzio et al., 2017; Clarke et al., 1977; Dahl-Jensen, 1989; Greve & Blatter, 2016). Thermal coupling can also lead to stream formation and oscillations, (e.g., Brinkerhoff & Johnson, 2015; Hindmarsh, 2009; MacAyeal, 1993; Payne, 1995).

The goal of the presented comparisons with the 2-D thermal model is not to mathematically quantify the effect of the horizontal advection term. Rather, our goal is to demonstrate the limitations of the 1-D analytical solution in a simple 2-D ice sheet profile and setting loose constraints beyond which the solution cannot be applied. Evidently, even in these simplest cases quantifying the impact of horizontal advection is not straightforward. Despite these limitations, we delineate the interior regions of the Greenland and Antarctic ice sheets where the effect of horizontal advection and strain heating are likely less than 2 K compared with the analytical solution. In all the comparisons between the analytical solution and the 2-D numerical solution shown in section 4, the horizontal surface velocity that corresponds to the location of a 2 K difference was more than 100 m/year. Owing to all the simplifications associated with the 2-D simulations, we chose a significantly more conservative range of 20 m/year for the limit of 2 K offset in the analytical temperature solution. Also, as shown in section 3, strain heating can be incorporated in the analytical solution by adding the depth-integrated strain heating to the geothermal heat flux up to driving stresses of ~50–60 kPa and produce basal temperatures within ~2 K of the actual value. Therefore, the boundaries marked in Figure 10 show the regions with both surface velocities less than 20 m/year and driving stresses smaller than ~60 kPa. Ice streams are excluded from the marked regions, because their inherent shelfy stream characteristic (MacAyeal, 1989) makes horizontal advection the dominant heat transport mechanism.
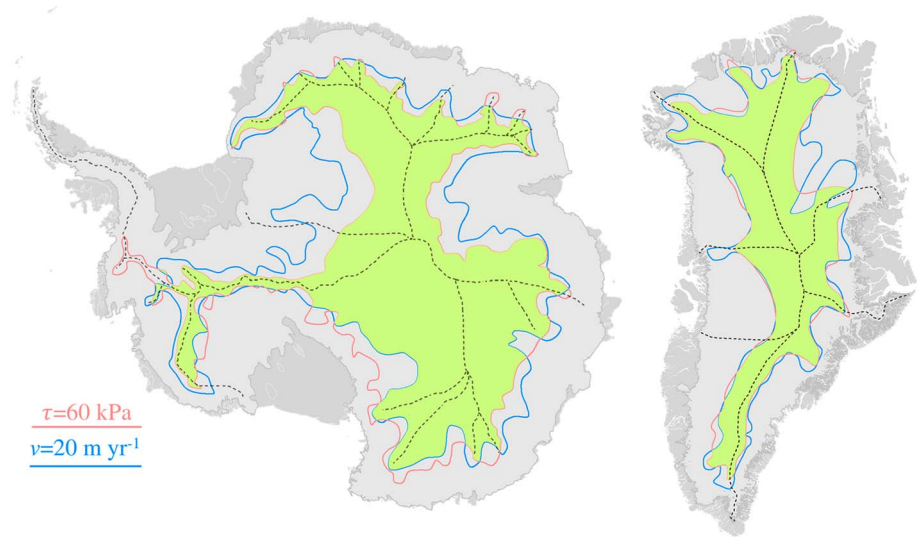
Figure 10. Approximate delineation of the regions where the analytical temperature solution can be used on the Greenland and Antarctic ice sheets with less than 2 K error (*green regions*). The boundaries mark the interior of both the driving stress of ∼60 kPa (*pink contour*) and surface velocity of 20 my/year (*blue contour*). Greenland and Antarctic velocities are from Joughin et al. (2010) and Rignot et al. (2011), respectively. The driving stresses for Greenland and Antarctica are calculated from surface digital elevation models of Bamber et al. (2013) and Fretwell et al. (2013), respectively, and all parameters are resampled to 10-km spatial resolution.

Throughout this study, the surface temperatures are chosen sufficiently low so as to avoid melting of the basal ice. However, assessing whether basal ice is at the pressure melting point can be done using our solution, since one can solve for the heat flux in (18) that is required for the basal ice to reach the pressure melting point, G_{pmp}, as

$$G_{pmp} = \frac{(T_{pmp} - T_s)\kappa(\gamma + 1)(-\phi)^{\frac{1}{\gamma+1}}}{\Gamma\left(\frac{1}{1+\gamma}, 0\right) - \Gamma\left(\frac{1}{1+\gamma}, -\phi H^{\gamma+1}\right)}. \tag{28}$$

The pressure melting temperature can be estimated by $T_{pmp} = 273.16 - \beta P$, where $P = \rho g H$ is the overburden pressure and β is the Clausius-Clapeyron constant of 9.8×10^{-8} kPa^{-1} (Cuffey & Paterson, 2010). If the sum of geothermal heat flux and strain heating close to the ice divide exceeds G_{pmp}, the melt rate, $\dot{b}$ can be estimated by

$$\dot{b} = \frac{G + G_s - G_{pmp}}{L_f \rho}, \tag{29}$$

where L_f is the latent heat of fusion (see Table 1). This can be used as a first-order approximation for assessing the thermal condition at the bed (e.g., Van Liefferinge & Pattyn, 2013) or find the minimum amount of heat required to thaw the bed at the radar-detected locations with basal thaw (e.g., Oswald et al., 2018). If it is concluded that the bed is at the pressure melting temperature, frictional heating can be readily added to the geothermal heat flux as $G_{sliding} = \tau \times v_{sliding}$.

6. Conclusion

We present a new analytical solution to the one-dimensional heat transport equation by parameterizing the vertical velocity profile as a power function. Temperatures from the analytical solution match numerical results obtained using vertical velocities derived from the SIA. We show that strain heating plays an important role in calculating the temperature profile of ice sheet interiors. We validate the approach suggested by Fowler (1992) that strain heating can be integrated at depth (G_s) and added to the geothermal heat flux at the bed. We show that with driving stresses of up to ∼50–60 kPa, the analytical solution with G_s overestimates the basal temperature by less than 2 K.

We evaluate errors in temperature estimates from the analytical solution arising from ignoring horizontal advection, by calculating the offset between the analytical solution and two-dimensional temperature estimates of a Vialov profile. The comparison results depend on various parameters such as surface mass balance rate, geothermal heat flux, and surface temperature lapse rate. The effect of horizontal heat advection is more pronounced on the englacial temperatures, but the basal temperatures from the analytical solution remain within 2 K of the numerically computed temperatures for a large portion of the ice sheet length. Finally, we mark approximate boundaries where the new analytical solution can be used with less than 2 K error in Greenland and Antarctica. The analytical solution presented can be used to validate temperature calculations from numerical ice sheet models.

References

Abramowitz, M., & Stegun, I. A. (1964). *Handbook of mathematical functions: With formulas, graphs, and mathematical tables* (Vol. 55). New York: Dover Publications.

Adalgeirsdottir, G., Aschwanden, A., Khroulev, C., Boberg, F., Mottram, R., Lucas-Picher, P., & Christensen, J. (2014). Role of model initialization for projections of 21st-century Greenland ice sheet mass loss. *Journal of Glaciology*, *60*(222), 782–794.

Amore, P. (2005). Asymptotic and exact series representations for the incomplete gamma function. *EPL (Europhysics Letters)*, *71*(1), 1.

Anandakrishnan, S., Blankenship, D. D., Alley, R. B., & Stoffa, P. (1998). Influence of subglacial geology on the position of a West Antarctic ice stream from seismic observations. *Nature*, *394*(6688), 62–65.

Aschwanden, A., Adalgeirsdottir, G., & Khroulev, C. (2013). Hindcasting to measure ice sheet model sensitivity to initial states. *The Cryosphere*, *7*(4), 1083.

Aschwanden, A., Bueler, E., Khroulev, C., & Blatter, H. (2012). An enthalpy formulation for glaciers and ice sheets. *Journal of Glaciology*, *58*(209), 441–457.

Bamber, J. L., Griggs, J. A., Hurkmans, R., Dowdeswell, J. A., Gogineni, S., Howat, I., et al. (2013). A new bed elevation dataset for Greenland. *The Cryosphere*, *7*(2), 499–510.

Bergman, T., Incropera, F., DeWitt, D., & Lavine, A. (2011). Fundamentals of heat and mass transfer. Hoboken, NJ: John Wiley.

Blatter, H., & Greve, R. (2015). Comparison and verification of enthalpy schemes for polythermal glaciers and ice sheets with a one-dimensional model. *Polar Science*, *9*(2), 196–207.

Bondzio, J. H., Morlighem, M., Seroussi, H., Kleiner, T., Rückamp, M., Mouginot, J., et al. (2017). The mechanisms behind Jakobshavn Isbræ's acceleration and mass loss: A 3D thermomechanical model study. *Geophysical Research Letters*, *44*, 6252–6260. https://doi.org/10.1002/2017GL073309

Boyce, W., DiPrima, R., & Haines, C. (1969). *Elementary differential equations and boundary value problems* (Vol. 9). New York: Wiley.

Brinkerhoff, D. J., & Johnson, J. V. (2013). Data assimilation and prognostic whole ice sheet modelling with the variationally derived, higher order, open source, and fully parallel ice sheet model VarGlaS. *The Cryosphere*, *7*, 1161.

Brinkerhoff, D. J., & Johnson, J. V. (2015). Dynamics of thermally induced ice streams simulated with a higher-order flow model. *Journal of Geophysical Research: Earth Surface*, *120*, 1743–1770. https://doi.org/10.1002/2015JF003499

Brooks, A., & Hughes, T. J. (1982). Streamline upwind/Petrov-Galerkin formulations for convection dominated flows with particular emphasis on the incompressible Navier-Stokes equations. *Computer Methods in Applied Mechanics and Engineering*, *32*(1-3), 199–259.

Clarke, G. K., Nitsan, U., & Paterson, W. S. (1977). Strain heating and creep instability in glaciers and ice sheets. *Reviews of Geophysics*, *15*(2), 235–247.

Cuffey, K. M., & Paterson, W. S. (2010). *The physics of glaciers*. Burlington, MA: Elsevier.

Cummings, E. M. (2016). Modeling the cryosphere with FEniCS. arXiv preprint arXiv:1609.02190.

Dahl-Jensen, D. (1989). Steady thermomechanical flow along two-dimensional flow lines in large grounded ice sheets. *Journal of Geophysical Research*, *94*(B8), 10,355–10,362.

Erokhina, O., Rogozhina, I., Prange, M., Bakker, P., Bernales, J., Paul, A., & Schulz, M. (2017). Dependence of slope lapse rate over the Greenland ice sheet on background climate. *Journal of Glaciology*, *63*(239), 568.

Ettema, J., Van den Broeke, M. R., Meijgaard, E., van, W. Berg, Box, J., & Steffen, K. (2010). Climate of the Greenland ice sheet using a high-resolution climate model—Part 1: Evaluation. *The Cryosphere*, *4*(4), 511–527.

Fowler, A. C. (1992). Modelling ice sheet dynamics. *Geophysical & Astrophysical Fluid Dynamics*, *63*(1-4), 29–65.

Fox Maule, C., Purucker, M., & Olsen, N. (2009). Inferring magnetic crustal thickness and geothermal heat flux from crustal magnetic field models. Copenhagen: Danish Climate Centre Report.

Fretwell, P., Pritchard, H. D., Vaughan, D. G., Bamber, J. L., Barrand, N. E., Bell, R., et al. (2013). Bedmap2: Improved ice bed, surface and thickness datasets for Antarctica. *The Cryosphere*, *7*, 375–393.

Gautschi, W. (1998). The incomplete gamma functions since tricomi, *Tricomi's ideas and contemporary applied mathematics, Atti dei Convegni Lincei, n. 147* (pp. 203–237). Roma: Accademia Nazionale dei Lincei Citeseer.

Greve, R., & Blatter, H. (2016). Comparison of thermodynamics solvers in the polythermal ice sheet model SICOPOLIS. *Polar Science*, *10*(1), 11–23.

Greve, R., & Hutter, K. (1995). Polythermal three-dimensional modelling of the Greenland ice sheet with varied geothermal heat flux. *Annals of Glaciology*, *21*, 8–12.

Hanna, E., Huybrechts, P., Janssens, I., Cappelen, J., Steffen, K., & Stephens, A. (2005). Runoff and mass balance of the Greenland ice sheet: 1958–2003. *Journal of Geophysical Research*, *110*, D13108. https://doi.org/10.1029/2004JD005641

Hindmarsh, R. C. (1999). On the numerical computation of temperature in an ice sheet. *Journal of Glaciology*, *45*(151), 568–574.

Hindmarsh, R. C. (2009). Consistent generation of ice-streams via thermo-viscous instabilities modulated by membrane stresses. *Geophysical Research Letters*, *36*, L06502. https://doi.org/10.1029/2008GL036877

Hindmarsh, R. C., Leysinger Vieli, G., & Parrenin, F. (2009). A large-scale numerical model for computing isochrone geometry. *Annals of Glaciology*, *50*(51), 130–140.

Hooke, R. L. (1981). Flow law for polycrystalline ice in glaciers' comparison of theoretical predictions, laboratory data, and field. *Reviews of Geophysics and Space Physics*, *19*(4), 664–672.

Hutter, K. (1983). *Theoretical glaciology; Material science of ice and the mechanics of glaciers and ice sheets*. Tokyo: D. Reidel Publishing Co., Terra Scintific Publishing Co.

Iken, A., & Bindschadler, R. A. (1986). Combined measurements of subglacial water pressure and surface velocity of Findelengletscher, Switzerland: Conclusions about drainage system and sliding mechanism. *Journal of Glaciology*, *32*(110), 101–119.

Jezek, K. C., Johnson, J., Drinkwater, M., Macelloni, G., Tsang, L., Aksoy, M., & Durand, M. (2015). Radiometric approach for estimating relative changes in intraglacier average temperature. *IEEE Transactions on Geoscience and Remote Sensing*, *53*(1), 134–143.

Joughin, I., Smith, B., Howat, I. M., Scambos, T., & Moon, T. (2010). *MEaSUREs Greenland ice sheet velocity map from InSAR data*. Boulder, CO: National Snow and Ice Data Center. https://doi.org/nsidc-0478.001

Larour, E., Morlighem, M., Seroussi, H., Schiermeier, J., & Rignot, E. (2012). Ice flow sensitivity to geothermal heat flux of Pine Island Glacier, Antarctica. *Journal of Geophysical Research*, *117*, F04023. https://doi.org/10.1029/2012JF002371

Larour, E., Seroussi, H., Morlighem, M., & Rignot, E. (2012). Continental scale, high order, high spatial resolution, ice sheet modeling using the Ice Sheet System Model (ISSM). *Journal of Geophysical Research*, *117*, F01022. https://doi.org/10.1029/2011JF002140

Logg, A., Mardal, K., & Wells, G. (2012). *Automated solution of differential equations by the finite element method: The FEniCS book* (Vol. 84). New York: Springer Science & Business Media.

MacAyeal, D. R. (1989). Large-scale ice flow over a viscous basal sediment: Theory and application to ice stream B, Antarctica. *Journal of Geophysical Research*, *94*(B4), 4071–4087.

MacAyeal, D. R. (1993). Binge/purge oscillations of the Laurentide Ice Sheet as a cause of the North Atlantic's Heinrich events. *Paleoceanography*, *8*(6), 775–784.

Morland, L. (1984). Thermomechanical balances of ice sheet flows. *Geophysical & Astrophysical Fluid Dynamics*, *29*(1-4), 237–266.

Nye, J. F. (1952). The mechanics of glacier flow. *Journal of Glaciology*, *2*(12), 82–93.

Oswald, G. K., Rezvanbehbahani, S., & Stearns, L. A. (2018). Radar evidence of ponded subglacial water in Greenland. *Journal of Glaciology*, *64*, 1–19.

Palmer, S., Dowdeswell, J. A., Christoffersen, P., Young, D. A., Blankenship, D. D., Greenbaum, J., et al. (2013). Greenland subglacial lakes detected by radar. *Geophysical Research Letters*, *40*, 6154–6159. https://doi.org/10.1002/2013GL058383

Payne, A. J. (1995). Limit cycles in the basal thermal regime of ice sheets. *Journal of Geophysical Research*, *100*(B3), 4249–4263.

Pettit, E. C., & Waddington, E. (2003). Ice flow at low deviatoric stress. *Journal of Glaciology*, *49*(166), 359–369.

Portnov, A., Vadakkepuliyambatta, S., Mienert, J., & Hubbard, A. (2016). Ice-sheet-driven methane storage and release in the Arctic. *Nature Communications*, *7*, 10,314.

Raymond, C. F. (1983). Deformation in the vicinity of ice divides. *Journal of Glaciology*, *29*(103), 357–373.

Rezvanbehbahani, S., Stearns, L. A., Kadivar, A., Walker, J., & van der Veen, C. J. (2017). Predicting the geothermal heat flux in Greenland: A machine learning approach. *Geophysical Research Letters*, *44*, 12,271–12,279. https://doi.org/10.1002/2017GL075661

Rignot, E., Mouginot, J., & Scheuchl, B. (2011). Ice flow of the Antarctic ice sheet. *Science*, *333*(6048), 1427–1430.

Robin, G. Q. (1955). Ice movement and temperature distribution in glaciers and ice sheets. *Journal of Glaciology*, *2*(18), 523–532. https://doi.org/10.3189/002214355793702028

Schlegel, N. J., Larour, E., Seroussi, H., Morlighem, M., & Box, J. E. (2015). Ice discharge uncertainties in Northeast Greenland from boundary conditions and climate forcing of an ice flow model. *Journal of Geophysical Research: Earth Surface*, *120*, 29–54. https://doi.org/10.1002/2014JF003359

Sergienko, O. V., Creyts, T. T., & Hindmarsh, R. C. (2014). Similarity of organized patterns in driving and basal stresses of antarctic and greenland ice sheets beneath extensive areas of basal sliding. *Geophysical Research Letters*, *41*, 3925–3932. https://doi.org/10.1002/2014GL059976

Siegert, M. J. (2000). Antarctic subglacial lakes. *Earth-Science Reviews*, *50*(1), 29–50.

Steffen, K., & Box, J. (2001). Surface climatology of the Greenland ice sheet: Greenland climate network 1995–1999. *Journal of Geophysical Research*, *106*(D24), 33,951–33,964.

Van Liefferinge, B., & Pattyn, F. (2013). Using ice-flow models to evaluate potential sites of million year-old ice in Antarctica. *Climate of the Past*, *9*(5), 2335–2345.

Van den Broeke, M. R., Bamber, J., Lenaerts, J., & Rignot, E. (2011). Ice sheets and sea level: Thinking outside the box. *Surveys in Geophysics*, *32*(4-5), 495–505.

Van der Veen, C. J. (2013). *Fundamentals of glacier dynamics*. Boca Raton FL: CRC Press.

Vialov, S. (1958). Regularities of lacial shields movement and the theory of plastic viscous flow. *Physics of the Movements of Ice IAHS*, *47*, 266–275.

Zotikov, I. (1986). *The thermophysics of glaciers*. Norwell, MA: Kluwer Academic Publishers.